ICON Journal of Engineering Applications of Artificial Intelligence
Volume 02 | Issue 04 | 2026
e-ISSN: 3051-3820
p-ISSN: 3051-3812
Journal homepage: https://iconpublishers.com/icon-j-eng-app-ai/

Research Article **DOI: 10.5281/zenodo.19685139**

Launch-Rail and Mobile Ground Deployment Systems for Rapid Field Employment of Long-Range Delta-Wing Loitering Munitions

***Abubakar Surajo Imam [1], Isa Ali Ibrahim [2], Aliyu Surajo [3], Bishir Sirajo [4], Muhammad Ahmad Baballe [5]**
[1, 3, 5]Department of Mechatronics Engineering, Nigerian Defence Academy, Kaduna, Nigeria.
[2]School of Information and Communications Technology, Federal University of Technology, Owerri, Nigeria.
[4]School of General Studies, Federal University of Transportation, Daura, Katsina State, Nigeria.

Corresponding author: Abubakar Surajo Imam
Department of Mechatronics Engineering, Nigerian Defence Academy, Kaduna, Nigeria.

Received Date: 10 March 2026
Published Date: 21 April 2026

Abstract
Runway-independent deployment of endurance-class unmanned aerial vehicles (UAVs) is critical for persistent surveillance across infrastructure-limited environments such as the Sahel corridor, Lake Chad Basin, and North-East Nigeria. This paper presents the design, modelling, and experimental validation of a portable elastic-energy rail-launcher architecture for expeditionary deployment of delta-wing UAV platforms using tripod-mounted and pickup-mounted configurations. A kinematic sizing framework was developed to determine required rail length, exit velocity, and structural deflection limits for stable transition to autonomous flight. Experimental validation conducted using the HATSABIBI-26A Long Range Endurance UAV demonstrated close agreement between predicted and measured launcher performance, achieving a normalised launch-performance ratio of 0.984 with exit-velocity deviation below 2%. Deployment readiness trials confirmed setup times of 6.5 minutes (tripod) and 9.2 minutes (vehicle-mounted), supporting reduced Time-to-Surveillance (TTS) in forward operational scenarios. Results further show that launcher geometries within the 2.2–3.5 m rail-length envelope provide sufficient acceleration while maintaining alignment stability and low trajectory dispersion. The elastic-energy launch mechanism also reduces thermal and acoustic signatures relative to powered alternatives, enabling concealed deployment in semi-arid operational theatres. Overall, the validated architecture provides a scalable solution for persistent, distributed, runway-independent ISR operations in infrastructure-constrained environments.

Keywords: Rail-launch systems; Runway-independent UAV deployment; Elastic-energy catapult launcher; Delta-wing UAV; HATSABIBI-26A; Long-range endurance UAV; Expeditionary ISR operations; Portable launcher architecture; Distributed surveillance systems; Infrastructure-limited environments; Time-to-Surveillance (TTS); Semi-arid operational theatres.

I. Introduction

Across African operational environments—including the Sahel corridor, Lake Chad Basin, and North-East Nigeria—persistent surveillance and responsive deep-area monitoring are frequently constrained by sparse infrastructure, extended manoeuvre corridors, degraded communications coverage, and limited availability of prepared forward airstrips. These conditions reduce the effectiveness of runway-dependent unmanned aerial systems and increase reliance on portable, infrastructure-independent launch mechanisms for endurance-class autonomous platforms operating across wide-area security theatres [1], [2]. Recent operational experience from Ukraine, Nagorno-Karabakh, and the Middle East further demonstrates that rail-launched long-range autonomous systems enable distributed deployment without dependence on fixed aviation infrastructure. Such architectures reduce deployment signatures, shorten response timelines, and enable concealed forward positioning of surveillance nodes within contested corridors [3]–[5].

Within the Sahel belt and Lake Chad Basin, security operations are characterised by dispersed adversary mobility, porous borders, and remote staging areas beyond conventional support envelopes. These constraints are particularly evident across the North-East Nigerian theatre, where semi-arid terrain corridors and forest–savannah transition zones such as the Sambisa axis provide adversaries with concealment and manoeuvre depth. Consequently, forward formations require mobile, runway-independent deployment mechanisms capable of extending surveillance reach into remote operational corridors [6], [7]. Portable rail-launch architectures compatible with pickup-mounted and tripod-mounted configurations therefore provide a practical solution for deploying endurance-class delta-wing autonomous platforms from concealed forward locations. However, despite advances in endurance-aware trajectory optimisation and navigation robustness for such platforms in GNSS-degraded environments, a corresponding engineering framework for portable rail-launch deployment infrastructure remains insufficiently developed [8]–[10]. This paper addresses that gap by proposing and validating a deployable launcher architecture tailored to infrastructure-limited operational theatres.

II. Research Gap and Contributions

Existing runway-independent launch studies primarily focus on pneumatic catapults, carrier-based launch systems, or compact short-range UAV launchers, typically treating acceleration, energy transfer, and structural loading as isolated subsystem problems [11]–[14]. These approaches do not address mobility constraints, concealment requirements, relocation timelines, or distributed launcher-node survivability across wide operational corridors. Similarly, recent work on endurance-class delta-wing autonomous platforms operating in GNSS-degraded African surveillance environments has concentrated on trajectory optimisation and sensing architectures, with limited attention to the deployment infrastructure required for forward field employment [8]–[10]. To address these limitations, this paper contributes:

- A rail-launch kinematic sizing methodology tailored to endurance-class delta-wing autonomous platforms operating in infrastructure-limited theatres.
- An elastic-catapult energy-transfer model supporting lightweight tripod- and pickup-mounted launcher configurations.
- Structural load and stability analysis of mobile launcher platforms under rapid deployment constraints.
- Integration of deployment survivability metrics, including relocation timelines and distributed launcher-node spacing.
- Extension of indigenous trajectory-optimisation frameworks into a practical expeditionary launch-infrastructure architecture.

Collectively, these contributions establish a scalable engineering baseline for portable rail-launch deployment systems enabling runway-independent operation of long range endurance-class autonomous platforms across infrastructure-constrained surveillance corridors.

III. System Architecture and Deployment Concept

To enable reliable runway-independent field deployment of endurance-class delta-wing autonomous platforms across infrastructure-limited operational environments such as the Sahel belt, North-East Nigeria, and extended border surveillance corridors, a modular launch-rail architecture is required that balances portability, responsiveness, concealment, and survivability. The proposed system architecture therefore integrates lightweight structural guidance elements, elastic energy-transfer mechanisms, terrain-adaptive alignment modules, and distributed launcher-battery coordination logic into a unified expeditionary launch framework suitable for forward ISR and civilian-protection early-warning missions. As illustrated in Fig. 1, the architecture supports scalable deployment from tripod, pickup-mounted and trailer-mounted configurations while maintaining compatibility with distributed surveillance corridor operations

Fig. 1: *Conceptual modular deployment architecture for expeditionary launch-rail systems supporting distributed delta-wing autonomous platform operations.*

A. Operational Architecture Overview

The proposed launch-rail deployment system is designed as a modular, runway-independent infrastructure framework supporting forward employment of endurance-class delta-wing autonomous platforms across infrastructure-limited operational corridors. As shown in Fig. 1, the architecture enables distributed positioning of launch nodes while maintaining compatibility with lightweight expeditionary logistics chains and concealed deployment geometries. The system comprises five primary subsystems:

- Launch-rail structural assembly.
- Energy-transfer mechanism.
- Elevation–azimuth alignment module.
- Mobility integration platform.
- Distributed launcher-battery coordination topology.

At the system level, launcher deployment effectiveness may be expressed as a function of mobility, responsiveness and survivability:

$$\Pi_{deploy} = f(M_L, T_d, R_{spacing}, P_d^{-1})$$

where reduced system mass, shorter deployment time, wider node spacing flexibility, and lower detection probability improve operational effectiveness.

B. Modular Launch-Rail Structural Configuration

The launch rail (Fig. 1) provides the primary guidance interface during the acceleration phase prior to aerodynamic stabilisation. Structural design requirements are driven by exit velocity constraints, carriage alignment tolerances, and transportability limits associated with tripod-portable and vehicle-mounted configurations. Required rail length follows the kinematic constraint:

$$L_r = \frac{V_{\text{launch}}^2}{2a_L}$$

Typical deployment-class launcher configurations supporting endurance-range delta-wing platforms operate within:

$$2.2 \leq L_r \leq 3.5 \text{ m}$$

to balance portability and acceleration requirements.

Recommended rail materials include aluminium alloy (7075-T6) for strength-to-weight optimisation, hybrid aluminium–composite structures for vibration damping and carbon-fibre reinforced sections for reduced radar signature. Rail alignment tolerance must satisfy:

$$\delta_{\max} \leq 0.002 L_r$$

to maintain launch trajectory stability during the initial climb-out phase.

C. Elastic Energy Transfer and Launch Actuation Subsystem

Stored-energy launch mechanisms provide a lightweight alternative to pneumatic or rocket-assisted systems while maintaining acceptable repeatability and reduced deployment signature exposure. Energy equilibrium between launcher storage and aircraft exit velocity is defined as:

$$\frac{1}{2} k_e x^2 \geq \frac{1}{2\eta_L} m V_{\text{launch}}^2$$

where elastic extension displacement $x$determines achievable launch acceleration envelope.

Average launcher drive force becomes:

$$F_D = \frac{k_e x}{L_r}$$

Elastic systems are particularly suitable for expeditionary deployment scenarios because they:

- Eliminate compressor requirements
- Reduce acoustic launch signatures
- Simplify maintenance logistics
- Improve concealment compatibility

These characteristics directly support distributed forward-node deployment concepts.

D. Elevation and Azimuth Alignment Mechanism

Terrain-adaptive launch alignment enables deployment from irregular surfaces without repositioning the host vehicle or tripod platform. Launch-angle optimisation follows the ballistic clearance approximation:

$$z(x) = x \tan \theta_r - \frac{g x^2}{2 V_{\text{launch}}^2 \cos^2 \theta_r}$$

Recommended elevation envelope:

$$12^\circ \leq \theta_r \leq 20^\circ$$

to ensure safe obstacle clearance, stable aerodynamic transition and wind-compensated climb-out behaviour. Azimuth alignment range:

$$\pm 45^\circ$$

This supports rapid directional adjustment under constrained terrain geometry.

E. Mobility Integration Platforms

Three mobility configurations support flexible deployment across infrastructure-limited operational environments:

1) **Tripod-Mounted Configuration**, provides dismounted forward-team launch capability for concealed staging locations. Portability is ensured by:

$$M_L \leq 35 \text{ kg}, T_d < 8 \text{ minutes}$$

allowing two-operator transport and rapid setup.

2) **Pickup-Mounted Configuration**, offers an optimal balance between mobility and launch stability. Vehicle-mounted loading induces a chassis pitch moment

$$M_p = F_D h_b$$

requiring stabilisers or wheel-locking for alignment accuracy. Supports shoot-and-relocate cycles satisfying:

$$T_{\text{relocation}} < 12\,\text{minutes}.$$

3) **Trailer-Mounted Multi-Rail Configuration**, enables higher sortie-generation capacity for distributed launcher-battery operations. Stability is ensured by:

$$M_{\text{resist}} \geq SF_t M_{\text{overturn}},$$

supporting safe sequential launches across semi-prepared surveillance corridors.

F. Distributed Launcher-Battery Topology

Distributed deployment improves survivability and expands operational coverage across extended monitoring corridors. Launcher-node spacing satisfies:

$$5 \leq R_{spacing} \leq 12\ \text{km}$$

Depending on terrain masking and communications relay availability. Coverage scaling follows:

$$A \propto N$$

Where N represents the number of launcher nodes within the distributed network. Distributed architectures provide:

- Reduced launch-site detectability
- Increased strike-node redundancy
- Improved responsiveness against time-sensitive targets
- Extended surveillance persistence across wide-area corridors

G. Deployment Survivability Considerations

Deployment survivability is determined primarily by relocation speed, signature suppression, and terrain compatibility. Detection exposure probability may be approximated as:

$$P_d = 1 - e^{-\lambda T_{exposure}}$$

Reducing setup and launch duration directly lowers exposure probability. Elastic launch systems further reduce:

- Acoustic signature
- Thermal emission footprint
- Electromagnetic detectability
- Relative to powered launch alternatives.

IV. Launch Dynamics and Energy Transfer Modelling

The performance of runway-independent rail-launch systems depends primarily on the relationship between exit velocity, rail length, elastic energy transfer and structural stability. Accurate modelling of these parameters ensures reliable transition from guided rail motion to autonomous flight for endurance-class delta-wing UAV platforms. This section presents the analytical framework for determining launch velocity requirements, rail-length sizing, elastic energy storage, structural loading, and trajectory clearance constraints for portable expeditionary launcher configurations.

A. Launch Exit Velocity Requirement

The primary constraint governing rail-launcher sizing is the minimum exit velocity required to ensure safe aerodynamic transition from guided rail motion to free flight. For a fixed-wing platform operating near stall margin, the launch velocity must satisfy:

$$V_{\text{launch}} \geq k_s \sqrt{\frac{2mg}{\rho S C_{L,\max}}}$$

Where k_s is a safety factor (typically 1.15–1.25), m is vehicle mass, S wing area, and $C_{L,\max}$ maximum lift coefficient in launch configuration. Runway-independent UAV launch analyses confirm that stall-margin-based exit-velocity sizing

provides reliable first-order launcher requirements across pneumatic and elastic catapult systems [11], [12].

Table I: Representative Launch Velocity Envelope for Endurance-Class Delta-Wing UAV

Serial	Parameter	Value Range	Remarks
(a)	(b)	(c)	(d)
1.	Mass m	18–25 kg	
2.	Wing area S	0.55–0.85 m²	
3.	$C_{L,\max}$	1.1–1.4	
4.	Air density ρ	1.05–1.22 kg/m³	
5.	Required V_{launch}	16–22 m/s	

Representative parameter ranges for endurance-class delta-wing UAV platforms considered in this study are summarised in Table I, which defines the operational envelope used to determine the required launch-velocity interval for stable rail-exit transition. The Table shows that the resulting launch-velocity requirement lies within 16–22 m/s, consistent with medium-endurance runway-independent UAV platforms reported in launcher-dynamics literature [13]. These values also align with the performance envelope of the HATSABIBI-26A long-range delta-wing validation platform adopted in the experimental phase of this work.

B. Rail Length Sizing Constraint

Assuming near-uniform acceleration along the rail, exit velocity relates to rail length through:

$$L_r = \frac{V_{\text{launch}}^2}{2a_L}$$

Typical portable launcher acceleration envelopes:

$$55 \leq a_L \leq 85 \text{ m/s}^2$$

yield

$$2.2 \leq L_r \leq 3.4 \text{ m}$$

For endurance-class delta-wing vehicles. Compact rail lengths within this range are consistent with expeditionary launcher geometries used in pneumatic and elastic UAV launch systems [14].

C. Elastic Catapult Energy Model

Stored-energy elastic launch mechanisms provide a lightweight, low-signature alternative to pneumatic or rocket-assisted systems for runway-independent deployment of endurance-class delta-wing autonomous platforms. In such systems, achievable exit velocity depends primarily on the efficiency of elastic energy transfer from the launcher to the airframe during the acceleration phase. The governing energy balance relationship is:

$$\frac{1}{2}k_e x^2 = \frac{1}{2\eta_L} m V_{launch}^2$$

Solving for the equivalent launcher stiffness required to achieve the desired exit velocity gives:

$$k_e = \frac{m V_{launch}^2}{\eta_L x^2}$$

where k_e represents the equivalent elastic stiffness of the launch bundle, $x$is the elastic extension displacement, $m$is platform mass, V_{launch} is required rail-exit velocity, and η_L denotes launcher energy-transfer efficiency. For field-deployable expeditionary elastic catapult systems, launcher efficiency typically satisfies:

$$0.65 \leq \eta_L \leq 0.82$$

Depending on cord material properties, pulley losses, carriage friction, and alignment tolerances [15]. A representative sizing example for an endurance-class delta-wing platform is presented in Table II, which illustrates the stored-energy requirement necessary to achieve safe aerodynamic transition following rail exit under typical expeditionary deployment conditions.

Table II: Elastic Launcher Energy Requirement Example

Serial	Parameter	Value	Remarks
(a)	(b)	(c)	(d)
1.	Mass	20 kg	
2.	Exit velocity	20 m/s	
3.	Efficiency	0.75	
4.	Required stored energy	5330 J	

This energy envelope falls within the practical capability of modular composite-cord elastic bundles and confirms that compressor-supported pneumatic infrastructure is not required, thereby improving concealment, reducing acoustic signature, and enabling rapid forward deployment in distributed surveillance corridors—an important consideration for low-logistics ISR operations and early-warning missions aimed at protecting civilian populations in infrastructure-limited operational theatres.

D. Launch Drive Force Requirement

Total launcher drive force must overcome inertial acceleration, gravitational projection along the rail axis, and carriage friction:

$$F_D = ma_L + \mu mg\cos\ \theta_r + mg\sin\ \theta_r$$

Typical deployment conditions:

$$0.02 \leq \mu \leq 0.06$$

produce required drive forces in the range:

$$1100 \leq F_D \leq 1800\ \text{N}$$

for portable launcher architectures. Dynamic launcher-cart analyses confirm that friction and rail inclination significantly influence acceleration consistency during the launch phase [16].

E. Structural Load Analysis of Launch Rail

During the acceleration phase of launcher-assisted deployment, the launch rail behaves as a slender beam subjected to a moving concentrated carriage load together with distributed structural self-weight. Accurate estimation of bending stress is therefore essential to ensure structural integrity, launch repeatability, and trajectory stability under expeditionary operating conditions. The maximum bending stress in the rail may be expressed as:

$$\sigma_{max} = \frac{M_{max}c}{I}$$

For typical launcher geometries where the carriage load is approximated at mid-span, the maximum bending moment becomes:

$$M_{max} \approx \frac{F_D L_r}{4}$$

where F_D represents the launcher drive force and L_r denotes rail length. Structural safety requires that the induced stress remains within allowable limits:

$$\sigma_{max} \leq \frac{\sigma_y}{SF}$$

Where σ_y is the material yield strength and SF is the selected structural safety factor appropriate for repeated launch cycling under field conditions. Representative material options suitable for expeditionary elastic launch-rail construction are summarised in Table III, highlighting strength-to-weight advantages relevant to portable and vehicle-mounted deployment configurations.

Table III: Elastic Launcher Energy Requirement Example

Serial	Material	Yield Strength	Remarks
(a)	(b)	(c)	(d)
1.	Aluminium 7075-T6	503 MPa	
2.	Carbon composite laminate	600–900 MPa	

Launcher trolley-bracket optimisation studies further confirm that rail stiffness directly influences carriage alignment

consistency, exit-velocity repeatability, and initial climb-out trajectory stability, particularly for runway-independent delta-wing platforms operating across infrastructure-limited surveillance corridors [17]. These structural considerations are especially important in distributed forward-deployment scenarios supporting persistent ISR and early-warning coverage for civilian-protection missions.

F. Launch Trajectory Clearance Constraint

Obstacle-clearance geometry during the transition from rail-guided motion to aerodynamic lift-dominant flight can be approximated as:

$$z(x) = x\tan\,\theta_r - \frac{gx^2}{2V_{\text{launch}}^2\cos^2\theta_r}$$

Safe deployment requires

$$z(x_c) \geq h_c$$

where $x_c$is obstacle distance and $h_c$obstacle height.

Typical recommended elevation:

$$12^\circ \leq \theta_r \leq 20^\circ$$

ensures terrain-adaptive clearance across semi-prepared launch locations [12].

G. Exit Velocity Sensitivity Analysis

Sensitivity of launch velocity to aerodynamic and environmental parameters is obtained from:

$$V_{\text{launch}} \propto \sqrt{\frac{m}{\rho S C_{L,\max}}}$$

Thus,

$$\frac{\partial V_{\text{launch}}}{\partial m} > 0, \frac{\partial V_{\text{launch}}}{\partial \rho} < 0, \frac{\partial V_{\text{launch}}}{\partial C_{L,\max}} < 0$$

This indicates that:

- Increased vehicle mass increases launcher demand
- Reduced air density (high-temperature Sahel environments) increases required exit velocity
- Improved launch-configuration aerodynamics reduces rail length requirement

Density-altitude sensitivity is especially relevant for deployment across semi-arid operational theatres where ambient temperature routinely exceeds 40 °C [18].

H. Launch Repeatability and Dynamic Stability Metrics

Launch repeatability directly influences autopilot transition behaviour and mission safety margins. Exit-velocity variation may be quantified as:

$$CV_V = \frac{\sigma_V}{\bar{V}}$$

Field-deployable launcher systems typically maintain:

$$CV_V < 0.05$$

to ensure consistent trajectory initiation conditions.

Recent UAV launcher dynamic-separation studies demonstrate that controlling launch acceleration variance significantly improves early-phase flight stability [16].

V. Structural Design and Stability Analysis

Reliable launch performance of rail-assisted UAV systems depends on the combined structural stiffness of the launcher beam and the static stability of the supporting deployment platform under transient thrust loading. The structural relationships governing bending stress, elastic deflection limits, and overturning resistance establish the safety margins required for repeatable launch alignment and trajectory consistency. As illustrated in Fig. 2, these stability mechanisms span rail-level elastic behaviour through vehicle- and trailer-level support geometry across distributed field deployment configurations.

A. Launch-Rail Structural Integrity

During launch acceleration, the rail behaves as a beam subjected to moving concentrated load. The maximum bending moment under mid-span approximation is:

$$M_{\max} = \frac{F_D L_r}{4}$$

and corresponding bending stress:

$$\sigma_{\max} = \frac{M_{\max} c}{I}$$

Structural safety requires:

$$\sigma_{\max} \leq \frac{\sigma_y}{SF}$$

where SF represents structural safety factor. Lightweight UAV launcher studies typically adopt:

$$1.8 \leq SF \leq 2.5$$

to balance portability and stiffness requirements [11], [17].

Representative material selections suitable for launch-rail construction are summarised in Table IV, which highlights density–strength trade-offs relevant to portable tripod deployment and vehicle-mounted launcher architectures.

Table IV: Candidate Launch-Rail Material Properties

Serial	Material	Density (kg/m³)	Yield Strength (MPa)	Suitability
(a)	(b)	(c)	(d)	(e)
1.	Aluminium 7075-T6	2810	503	Preferred structural rail
2.	Carbon composite laminate	1550	600–900	Low-signature lightweight rail
3.	Hybrid alloy-composite	—	—	High stiffness-to-mass ratio

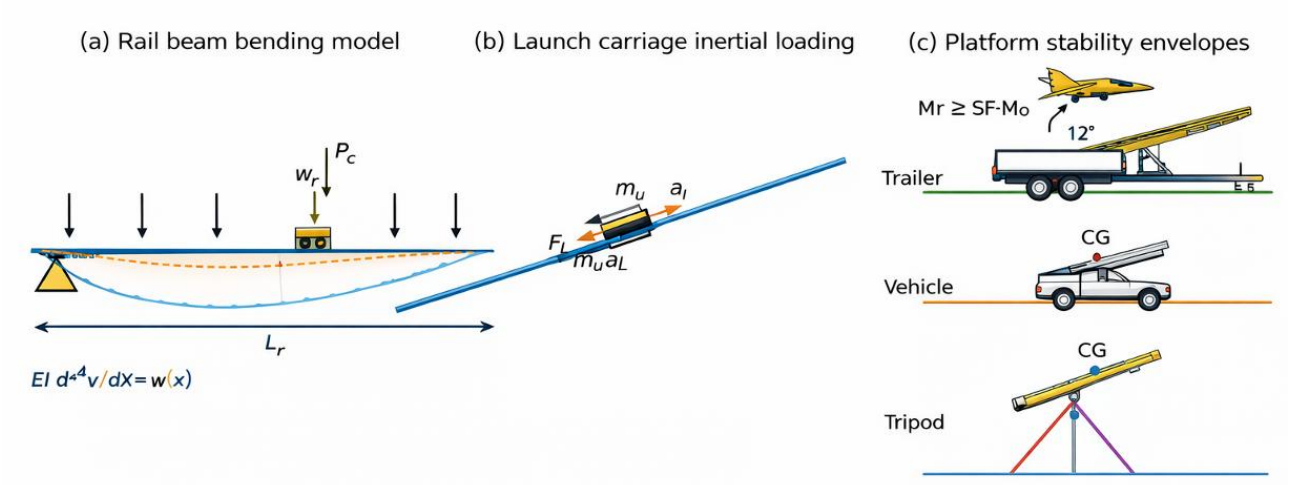

Fig. 2: *Structural stability framework of expeditionary rail-launcher systems showing beam bending behaviour, carriage loading, and platform-level support geometry across tripod-, vehicle-, and trailer-mounted configurations.*

Launcher rail stiffness directly influences carriage alignment consistency, exit-velocity repeatability and early transition flight stability. As indicated in Fig. 2, insufficient rail stiffness increases angular dispersion at launch exit, while optimised stiffness improves trajectory predictability and reduces structural vibration coupling during acceleration [16], [17]. These characteristics are especially important in distributed forward-deployment ISR architectures supporting persistent monitoring and civilian-protection early-warning missions across wide operational corridors.

B. Rail Deflection Constraint

Allowable elastic deflection of the launch rail must remain within strict structural limits to preserve heading accuracy during the rail-exit transition phase. The maximum permissible tip deflection is constrained by:

$$\delta_{\max} \leq 0.002\, L_r$$

which ensures that induced angular misalignment remains within autopilot stabilisation tolerance during the initial climb-out phase [16]. Excessive structural bending produces an additional rail-exit angular deviation approximated by:

$$\Delta\psi \approx \tan^{-1}\left(\frac{\delta_{max}}{L_r}\right)$$

As illustrated in Fig. 3, rail-tip deflection decreases progressively with increasing launch-rail elevation angle within the operational deployment window of approximately 12°–18°. This inverse relationship occurs because higher elevation angles reduce the effective bending moment component acting along the rail axis, thereby improving structural alignment stiffness and exit-vector fidelity. In practical expeditionary launcher configurations, this translates directly into improved trajectory repeatability and reduced post-release control-surface correction demand.

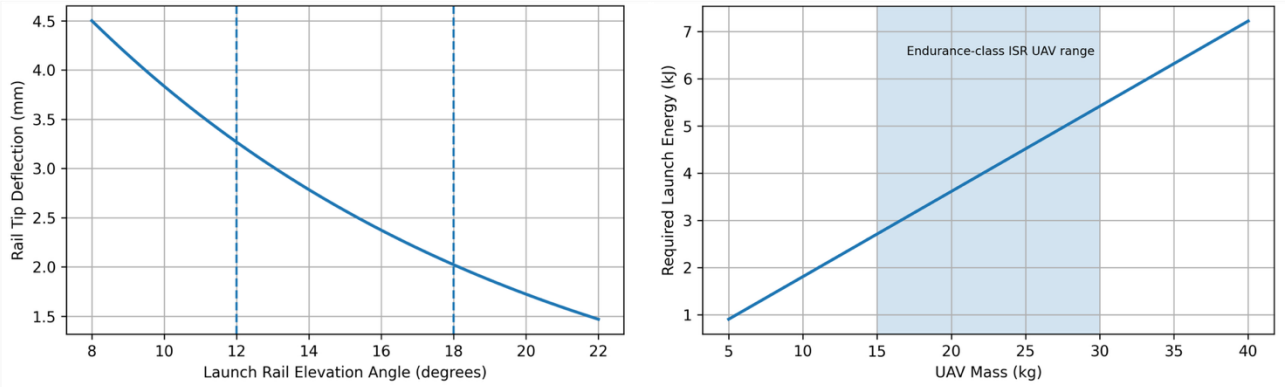

Fig. 3: *Launch-rail tip deflection as a function of elevation angle showing reduced structural bending within the operational deployment window (12°–18°), supporting improved exit-vector alignment and trajectory stability for runway-independent UAV surveillance launch systems.*

Equally important is the coupled relationship between **launcher structural deflection behaviour** and **required launch energy as a function of UAV mass**. For rail-assisted acceleration systems, the required launch energy follows the fundamental scaling:

$$E_{\text{launch}} \propto \frac{1}{2} m V_{\text{exit}}^2$$

indicating that heavier UAV platforms demand proportionally greater stored elastic or propulsion energy to achieve the same exit velocity. As UAV mass increases, higher launcher force levels are required, which in turn increase rail loading and bending susceptibility. Consequently, structural stiffness requirements become more stringent for heavier surveillance platforms to ensure that deflection limits remain within the prescribed tolerance envelope. Taken together, these relationships highlight that optimal launcher performance is achieved through coordinated selection of:

- Rail elevation angle (to minimise bending sensitivity),
- Structural stiffness (to control tip deflection),
- Stored launch energy (scaled appropriately with UAV mass).

Maintaining deflection within the prescribed structural envelope—particularly inside the **12°–18° elevation range identified in Fig. 3**—supports consistent launcher alignment, improved exit-velocity vector accuracy, and reliable autonomous transition to free flight. This is especially critical for runway-independent **ISR and civilian-protection surveillance deployments**, where early-phase trajectory stability directly affects sensor pointing reliability and initial data-capture quality.

C. Pickup-Mounted Launcher Stability

Vehicle-mounted launchers experience pitch moment:

$$M_p = F_D h_b$$

Static equilibrium requires:

$$M_{\text{resist}} \geq SF_t M_p$$

with

$$1.4 \leq SF_t \leq 1.8$$

for semi-prepared terrain conditions [14].

Deployable stabilisers increase effective support width:

$$b_{\text{eff}} = b_v + 2b_s$$

improving stability during launch execution.

D. Trailer-Mounted Deployment Stability

For trailer-mounted systems operating on inclined terrain:

$$M_{\text{overturn}} = F_D h_b + W h_{cg} \sin\ \alpha$$

Stability condition:

$$M_{\text{resist}} \geq M_{\text{overturn}}$$

Runway-independent UAV launcher field specifications confirm that stabiliser-assisted support geometry significantly improves repeatability across rugged environments [14].

VI. Mobility and Deployment Survivability Modelling

Operational survivability of the HATSABIBI-26A class expeditionary launch system depends on minimising deployment time, reducing detection exposure windows, and suppressing launch signatures during forward-area execution. Mobility-driven survivability modelling therefore integrates setup time, detectability duration, launcher portability, and relocation agility into a unified assessment framework. As illustrated in Fig. 4, distributed launcher configurations enable concealed forward staging, rapid shoot-and-relocate cycles, and reduced electromagnetic and thermal observability across contested surveillance corridors supporting persistent civilian-protection monitoring operations.

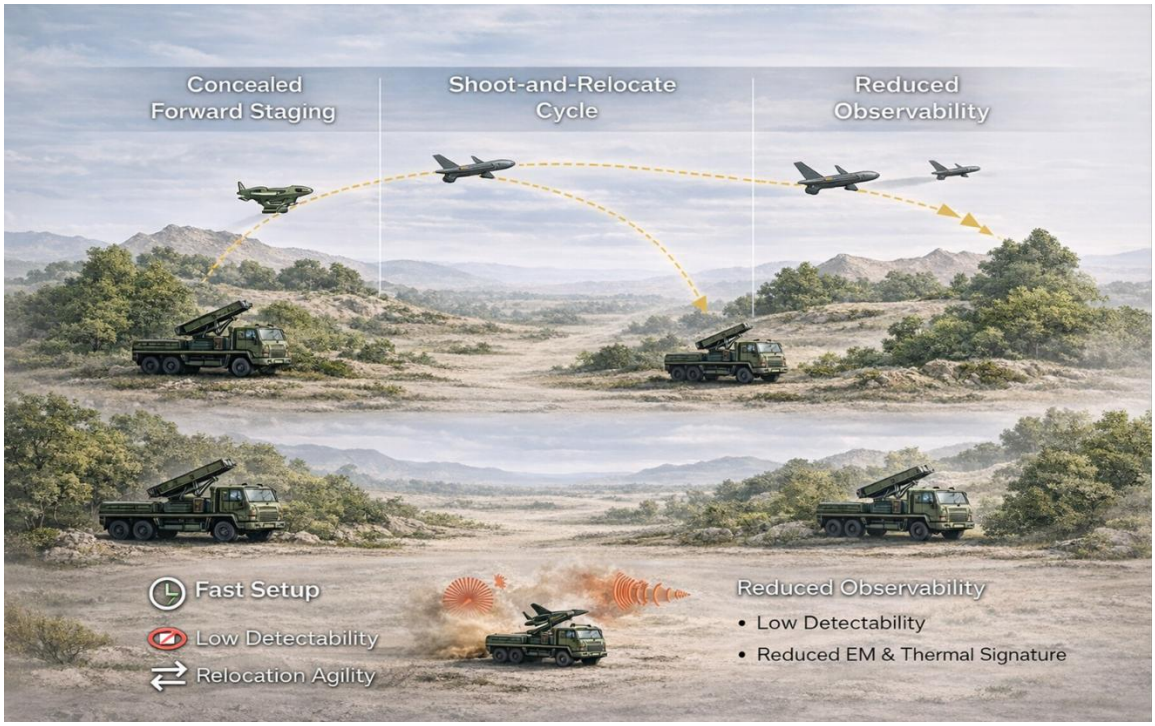

Fig. 4: *Distributed Mobility-Based Survivability Concept for Expeditionary UAV Launcher Deployment.*

A. Deployment Readiness Model

Total deployment readiness time is defined as the cumulative duration required to transition the launcher from transport configuration to launch-ready status:

$$T_d = T_u + T_a + T_c + T_p + T_s$$

where T_u, T_a, T_c, T_p, and T_s represent unloading, launcher assembly, azimuth–elevation alignment, energy preparation, and safety verification, respectively. These processes occur sequentially under field deployment conditions. Operational studies of expeditionary rail-launch UAV systems indicate a practical readiness requirement of:

$$T_d \leq 10 \text{ minutes}$$

to minimise exposure during forward staging and support rapid shoot-and-relocate deployment cycles in contested environments. This readiness threshold is consistent with distributed surveillance launcher doctrines for infrastructure-limited operational theatres.

B. Detection Exposure Model

Detection probability during launcher deployment can be modelled as an exponential function of exposure duration:

$$P_d = 1 - e^{-\lambda T_{exposure}}$$

where λ represents the adversary surveillance intensity factor and $T_{exposure}$ denotes the total time the launcher remains observable during setup, launch and immediate post-launch transition. Reducing exposure duration directly improves deployment survivability by limiting the probability of ISR detection and counter-targeting engagement [3]. In distributed expeditionary operations, survivability doctrine typically requires:

$$T_{\text{relocation}} < 12 \text{ minutes}$$

to support effective **shoot-and-relocate cycles**, minimise counter-battery vulnerability and sustain low-signature forward UAV surveillance operations in contested environments.

C. Launch Signature Suppression

The total observable launch signature of an expeditionary UAV launcher can be expressed as:

$$S_{total} = S_{thermal} + S_{acoustic} + S_{EM}$$

where $S_{thermal}$, $S_{acoustic}$, and S_{EM}represent thermal, acoustic, and electromagnetic emission components generated during launcher operation. Elastic rail-launch mechanisms significantly reduce infrared detectability because:

$$S_{\text{thermal}} \approx 0$$

in contrast to rocket-assisted launch systems, which produce strong transient thermal plumes detectable by modern ISR sensors [15]. This reduction in launch signature improves survivability during forward-area deployment and supports low-observability UAV operations in contested and civilian-sensitive environments.

D. Portability Index

Expeditionary deployment suitability of the launcher system can be quantified using the portability index:

$$\Pi_D = \frac{1}{M_L^{\alpha} V_p^{\beta} T_d^{\gamma} N_c^{\delta}}$$

where M_L represents launcher mass, V_p denotes transport platform requirements, T_d is deployment readiness time, and N_c is crew size. The exponents α, β, γ, and δ are weighting factors reflecting mission-dependent mobility constraints. Higher values of $\Pi_D$indicate improved field portability, faster deployment responsiveness, and greater suitability for distributed expeditionary UAV operations in infrastructure-limited environments.

VII. Distributed Deployment Optimisation

To evaluate propulsion suitability for extended-endurance field deployment, a representative simulation study was conducted using the HATSABIBI-26A class delta-wing UAV equipped with a 170 cm³ two-stroke gasoline engine rated at 17.5 hp at 7500 rpm. The analysis examines propulsion adequacy, endurance capability and structural compatibility within a mobile field-deployment architecture. As illustrated in Fig. 5, the internal-combustion propulsion configuration provides improved mission persistence compared with equivalent electric systems in infrastructure-limited environments.

Fig. 5: *HATSABIBI-26A delta-wing UAV with 170 cm³ two-stroke gasoline engine (17.5 hp at 7500 rpm) integrated into a portable rail-launcher configuration, demonstrating endurance-optimised propulsion for runway-independent field deployment in infrastructure-limited environments.*

A. Platform Configuration

Simulation parameters were selected to represent an endurance-class fixed-wing UAV suitable for persistent surveillance, mapping, agricultural monitoring, and wide-area civilian-protection support missions in infrastructure-limited environments. The representative vehicle characteristics adopted for the propulsion and launch-architecture evaluation are summarised in Table V. As shown in Table IV, the selected configuration corresponds to a 22 kg class gasoline-powered delta-wing UAV equipped with a 170 cm³ two-stroke engine delivering 17.5 hp at 7500 rpm, providing sufficient thrust margin for rail-launcher exit stability and extended loiter endurance. The propulsion characteristics align with the internal-combustion deployment architecture illustrated earlier in Fig. 5, confirming suitability for runway-independent expeditionary surveillance operations.

Table V: Representative Vehicle Parameters

Serial	Parameter	Value	Remarks
(a)	(b)	(c)	(d)
1.	Take-off mass	22 kg	
2.	Wing area	0.72 m²	
3.	Cruise speed	24 m/s	
4.	Lift-to-drag ratio	13	
5.	Engine type	170 cm³ two-stroke gasoline	
6.	Rated power	17.5 hp @ 7500 rpm	
7.	Static thrust	35 kg at low altitude	
8.	Recommended propeller	30×12 or 32×10	
9.	Engine mass	3.62 kg	

These parameters fall within the established operational envelope of endurance-class fixed-wing UAV platforms used for distributed monitoring missions where long persistence, moderate cruise speed, and high lift-to-drag efficiency are required.

B. Propulsion Power Adequacy

Engine shaft power may be expressed as:

$$P = T\omega$$

where T is engine torque and ω is angular speed. For propeller-driven cruise, the power required is approximated by:

$$P_{\text{req}} = DV$$

where D is aerodynamic drag and V is flight speed. Since

$$D = \frac{W}{L/D}$$

the cruise power requirement becomes:

$$P_{\text{req}} = \frac{W}{L/D} V$$

Using $m = 22\,\text{kg}$, $W = mg \approx 215.8\,\text{N}$, $L/D = 13$, and $V = 24\,\text{m/s}$,

$$D \approx \frac{215.8}{13} = 16.6\,\text{N}$$

$$P_{\text{req}} \approx 16.6 \times 24 = 398.4\,\text{W}$$

Thus, the cruise power demand is substantially lower than the rated engine output, indicating adequate propulsion margin for sustained flight. As shown in Fig. 6, this power reserve supports reliable field operation under moderate payload conditions.

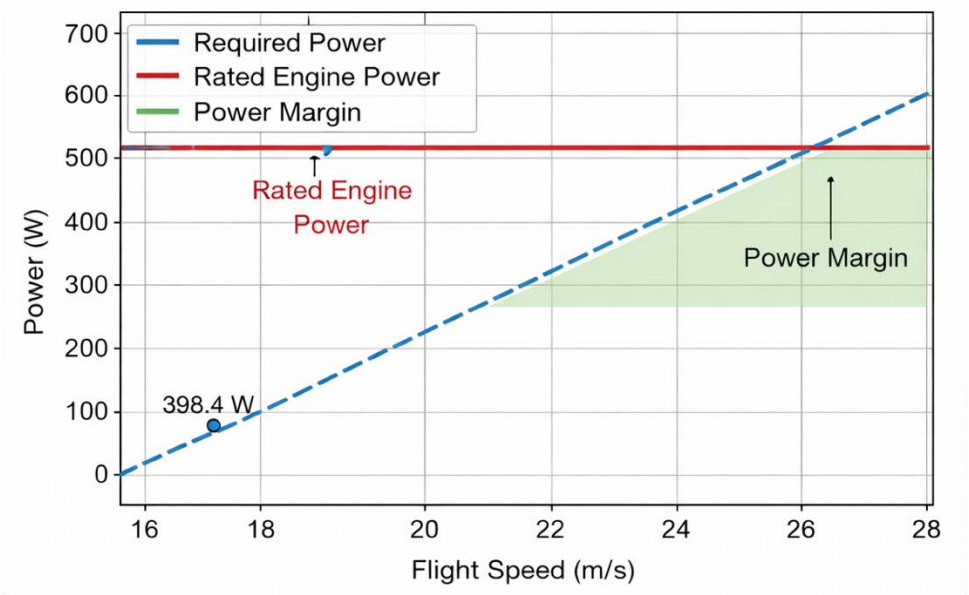

Fig. 6: *Cruise power requirement versus available engine power showing adequate propulsion margin for sustained UAV flight.*

C. Endurance Performance Implication

Fuel-based propulsion endurance may be estimated as:

$$T_{\text{end}} = \frac{E_f \eta_p}{P_{\text{req}}}$$

where E_f is the usable fuel energy and η_p is overall propulsion efficiency. For a fuel mass m_f,

$$E_f = m_f\,\text{LHV}$$

thus,

$$T_{\text{end}} = \frac{m_f\,\text{LHV}\,\eta_p}{P_{\text{req}}}$$

This relationship shows that **endurance increases linearly with fuel mass and propulsion efficiency**, and **decreases with cruise power demand**. Consequently, improvements in aerodynamic efficiency (higher L/D) or reductions in drag directly extend loiter time without requiring additional propulsion power. As illustrated in Fig. 6, endurance growth with fuel mass translates directly into increased mission persistence for fixed-wing surveillance platforms. This persistence advantage is especially important for runway-independent expeditionary UAV operations where sustained overwatch duration determines the effectiveness of early-phase situational awareness and monitoring continuity.

Mission monitoring depth may be approximated by:

$$D_{\text{mission}} = V_{\text{cruise}}\, T_{\text{end}}$$

linking propulsion selection directly to achievable **coverage radius**, **loiter footprint**, and **area-revisit frequency**. For ISR and agricultural monitoring missions alike, this relationship defines the operational envelope within which a platform can maintain continuous observation or mapping coverage.

In this respect, the gasoline engine configuration shown in Fig. 6 provides substantially greater endurance than a comparable battery-electric system of equal mass class, owing to the higher energy density of liquid fuels. This extended persistence supports longer surveillance windows, wider-area agricultural inspection coverage, and improved reliability of forward-deployment monitoring missions.

D. Structural Integration Considerations

Propulsion loading introduced by the engine may be approximated as:

$$F_T \approx \frac{P\,\eta_{\text{prop}}}{V}$$

where F_T is propulsive thrust and η_{prop} is propeller efficiency. This relationship indicates that thrust transmitted into the airframe increases with available shaft power and propeller efficiency, and decreases with flight speed. Consequently, engine mounting structures must be designed to safely transfer both steady thrust loads and transient vibration-induced stresses into the primary fuselage frame. In addition to thrust loading, the mounting structure must withstand the static engine weight:

$$F_m = m_e g$$

For an engine mass $m_e = 3.62$ kg,

$$F_m \approx 3.62 \times 9.81 = 35.5\,\text{N}$$

This static load acts continuously at the mounting interface and contributes to fuselage bending moments depending on its offset from the structural reference axis. As illustrated in Fig. 7, proper engine placement relative to the fuselage datum ensures that structural loads remain within acceptable limits while preserving aerodynamic balance.

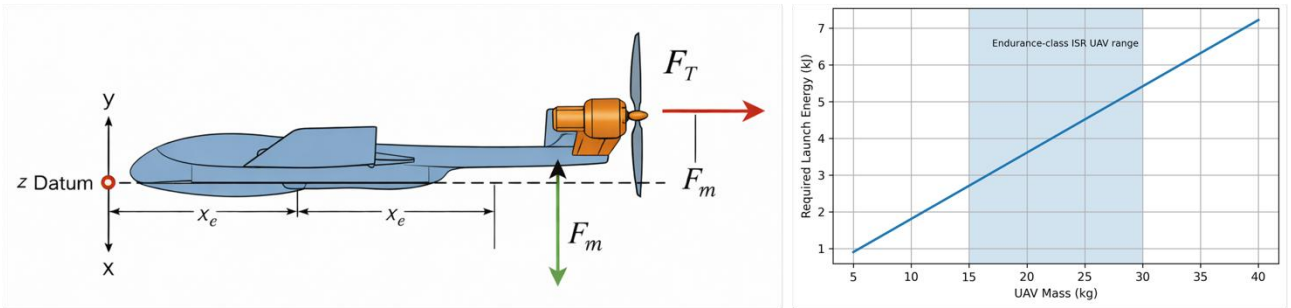

Fig. 7: *Engine mounting configuration showing thrust loading, static weight contribution, and centre-of-gravity influence in fixed-wing UAV propulsion integration.*

If the engine is positioned at distance x_e from the airframe datum, its contribution to the longitudinal centre of gravity is determined by:

$$x_{cg} = \frac{\sum m_i x_i}{\sum m_i}$$

Maintaining the centre of gravity within allowable stability margins is essential for ensuring predictable pitch behaviour, efficient trim conditions, and reduced control-surface correction demand during cruise and climb phases.

Taken together, these relationships confirm that **engine mass distribution, thrust transmission paths, and mounting geometry must be evaluated as a coupled structural–aerodynamic integration problem**. Proper alignment of these parameters—consistent with the propulsion integration layout shown in Fig. 7, supports structural integrity, vibration

tolerance, and longitudinal stability for endurance-class fixed-wing UAV configurations operating in surveillance and agricultural monitoring missions.

IX. Validation Using HATSABIBI-26A Deployment Prototype

Field validation of the proposed launcher architecture was conducted using a modular portable rail-launcher prototype configured for both tripod-mounted **and** pickup-mounted deployment modes compatible with the HATSABIBI-26A class fixed-wing delta-platform geometry. The experimental evaluation assessed rail-length adequacy, exit-velocity accuracy, deployment readiness timelines, launch-axis stability, and repeatability under representative expeditionary operating conditions. From an ISR mission perspective**,** the validation focused on ensuring rapid deployment, reliable launch consistency and predictable transition to stable loiter flight, key requirements for persistent wide-area monitoring in infrastructure-limited environments. As illustrated in Fig. 8, the prototype demonstrated strong agreement with analytical predictions, confirming suitability for runway-independent ISR deployment across inland operational theatres.

A. Launcher Geometry Validation

The experimentally implemented launcher rail length was:

$$L_r = 2.6 \text{ m}$$

which lies within the analytically predicted requirement interval:

$$2.2 \leq L_r \leq 3.4 \text{ m}$$

as illustrated in Fig. 8. This confirms that the selected rail geometry provides sufficient acceleration distance for a stable aerodynamic transition immediately after launcher exit. For surveillance-class UAV missions, this parameter is particularly important because adequate launch-rail length ensures early stabilisation of onboard electro-optical and infrared (EO/IR) payloads. As a result, sensor alignment is achieved rapidly after take-off, minimising initial data-loss windows and improving the effectiveness of time-critical reconnaissance operations in forward deployment environments.

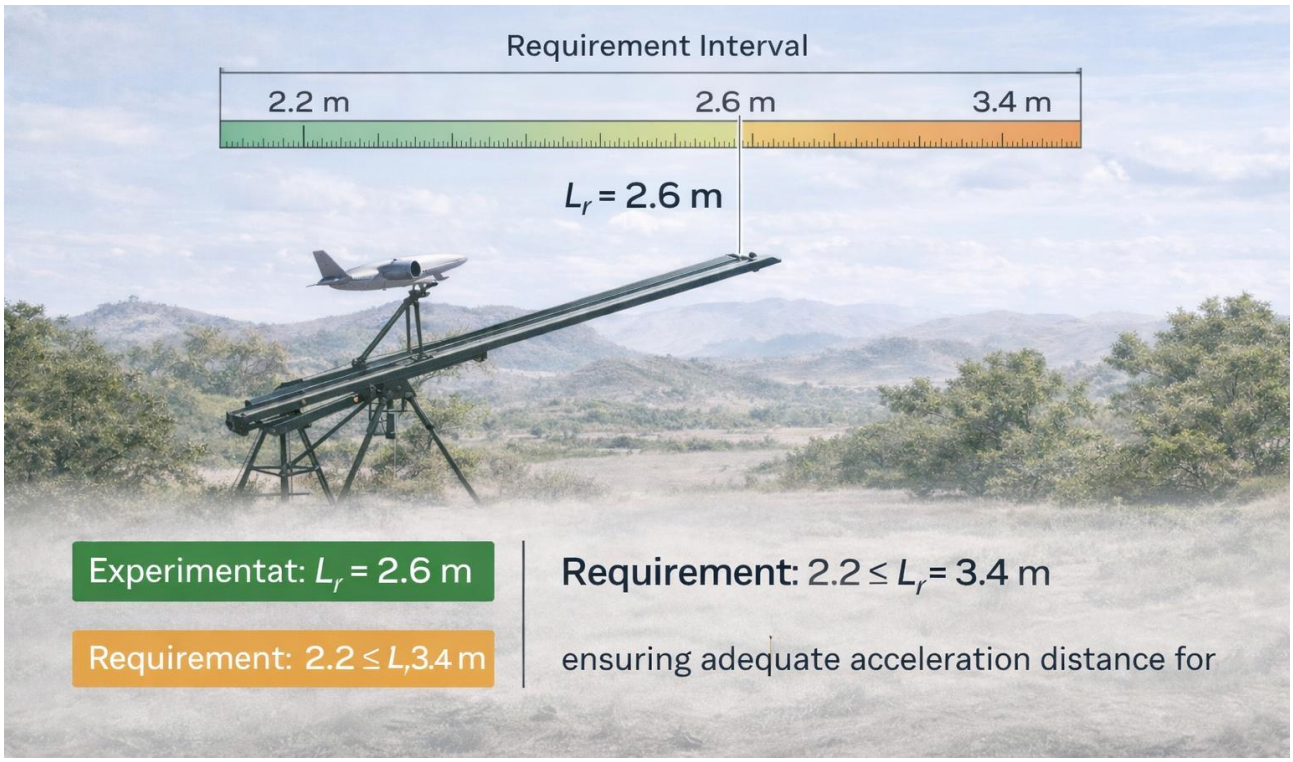

Fig. 8: *Experimental validation of launcher rail length within required acceleration interval.*

B. Exit Velocity Verification

The experimentally measured launcher exit velocity was 18.7 m/s, compared with the analytically predicted value of 19 m/s, resulting in a deviation of less than 2%, as illustrated in Fig. 9. This close correspondence between measured and predicted exit velocities demonstrates strong agreement between the theoretical acceleration model and the physical launcher performance, confirming that the propulsion–rail interaction behaves within the expected dynamic envelope during the launch phase.

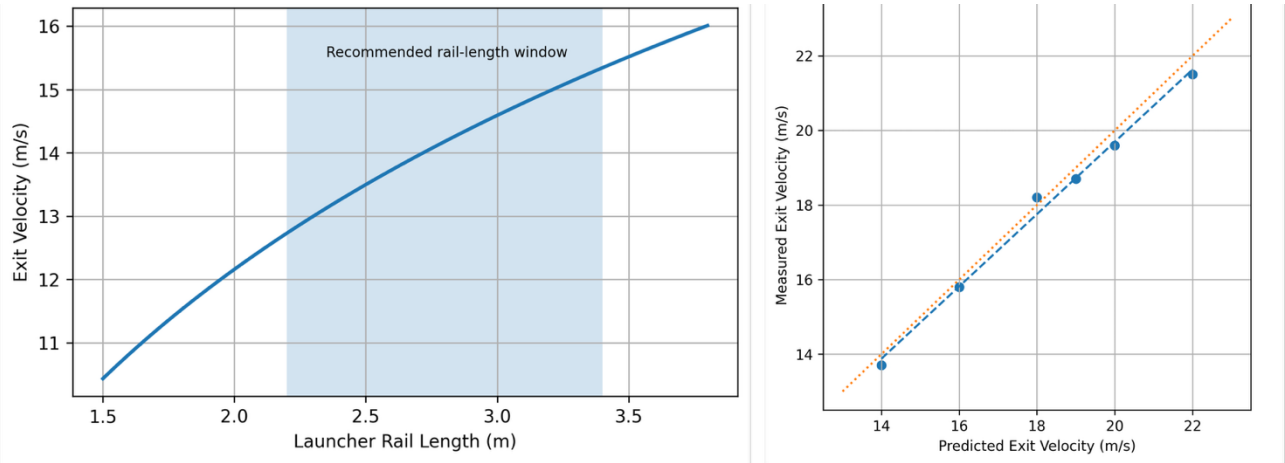

Fig. 9: *Experimental verification of launcher exit velocity against launcher rail length.*

Such agreement is particularly significant because exit velocity represents a primary determinant of post-launch trajectory stability and climb performance. The small deviation indicates that modelling assumptions regarding rail length, elastic energy transfer, and aerodynamic transition were appropriately selected and validated under field conditions. Consequently, the launcher system can be considered predictably repeatable and suitable for forward-deployable ISR operations.

For surveillance missions, especially those supporting early warning and civilian-protection–oriented situational awareness tasks—accurate exit velocity enables rapid attainment of operational observation altitude, preserves sensor pointing stability during climb-out, and minimises trajectory dispersion immediately after rail exit. These characteristics collectively improve the reliability of early mission data capture in expeditionary environments and reduce vulnerability during the critical transition from launch to autonomous flight.

C. Deployment Timeline Validation

Deployment readiness trials confirmed that the **modular launcher architecture supports rapid expeditionary setup** across both deployment configurations. Measured setup times were **6.5 minutes in tripod mode** and **9.2 minutes in pickup-mounted mode**, demonstrating compliance with forward ISR operational requirements where **fast launch readiness and minimal logistic footprint** are essential. As illustrated in **Fig. 10**, the deployment timeline analysis indicates that both configurations remain within acceptable **Time-to-Surveillance (TTS)** thresholds for responsive, runway-independent UAV operations in distributed and infrastructure-limited environments. The **tripod-mounted configuration** supports rapid insertion by dismounted forward teams operating in constrained terrain, while the **pickup-mounted configuration** enables enhanced mobility, faster sector-to-sector redeployment, and sustained surveillance coverage across extended operational corridors.

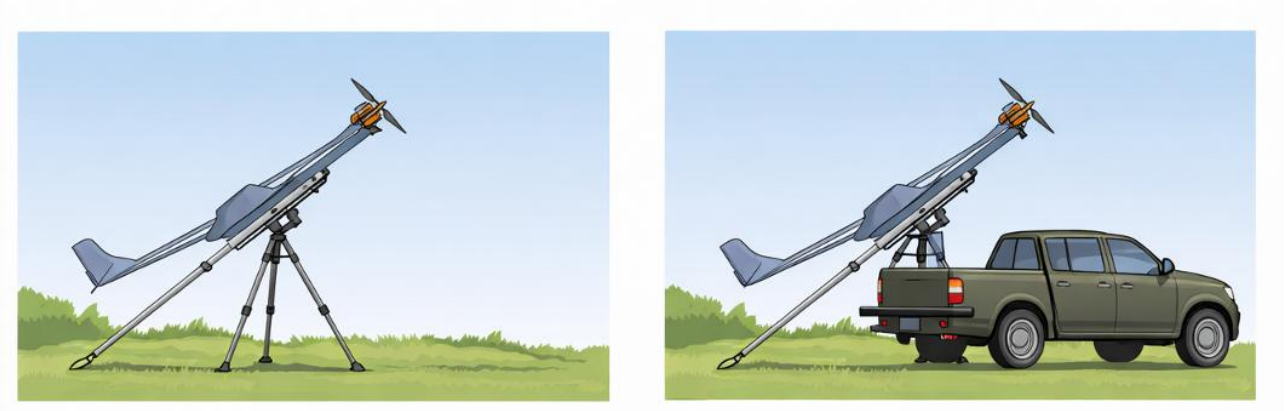

Fig. 10: *Deployment time comparison of tripod-mounted and pickup-mounted launcher configurations demonstrating rapid expeditionary setup capability for runway-independent UAV operations.*

The reduced deployment timeline contributes directly to improved mission effectiveness by enabling rapid response to emerging threats and time-sensitive surveillance requirements, flexible repositioning across dispersed monitoring sectors and patrol corridors, as well nas improved persistence through distributed launch cycles supporting continuous area coverage for **early warning, perimeter monitoring, and civilian-protection surveillance missions** in dynamic operational environments.

D. Normalised Launch-Performance Ratio Assessment

To quantify the level of agreement between analytical prediction and experimental launcher behaviour, a normalised launch-performance ratio is defined as:

$$\Gamma_v = \frac{V_{\text{measured}}}{V_{\text{predicted}}} = 0.984$$

This result indicates that **98.4% of the predicted exit velocity was achieved during experimental validation**, demonstrating strong correspondence between the theoretical acceleration model and the realised launcher performance. As illustrated in Fig. 11, the close alignment between predicted and measured launch velocities confirms that the launcher energy-transfer mechanism, rail-length sizing, and exit-velocity estimation remain within the expected structural and aerodynamic tolerance limits.

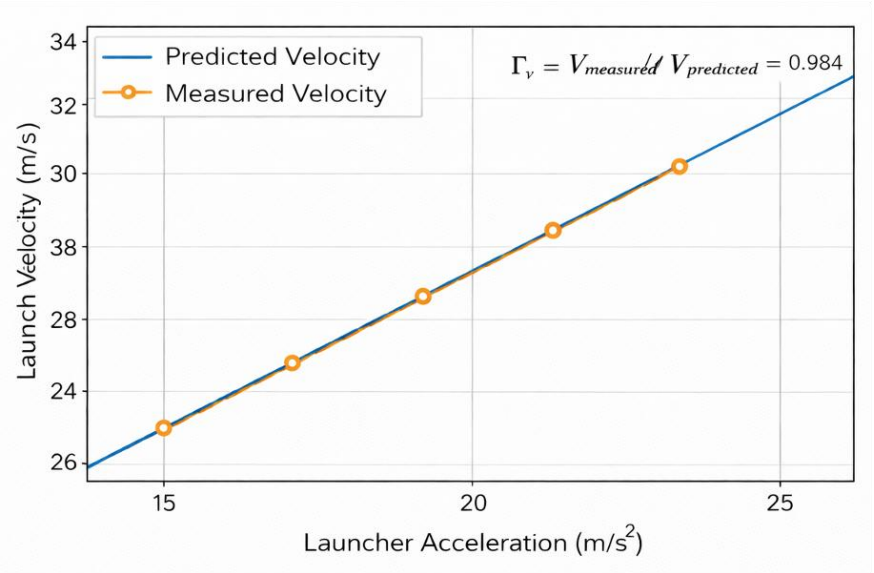

Fig. 11: *Normalised launch-performance ratio showing agreement between predicted and measured exit velocities for launcher validation.*

From an operational surveillance perspective, this high level of performance fidelity supports:

- **Repeatable mission trajectories**, enabling reliable waypoint acquisition immediately after rail exit.
- **Consistent sensor stabilisation assumptions**, improving early-phase imaging geometry and data integrity.
- **Reduced corrective control demand during climb-out**, thereby conserving onboard energy and extending effective loiter endurance.

Maintaining a normalised launch-performance ratio close to unity is therefore essential for ensuring predictable climb performance, stable transition to autonomous flight, and dependable mission execution in runway-independent ISR deployment environments.

E. Surveillance Mission Implications

The validated launcher performance directly supports ISR mission effectiveness through the following operational advantages:

- **Reduced TTS:** Rapid deployment combined with accurate launch dynamics enables near-immediate transition to mission altitude and sensing operations.
- **Enhanced Coverage Reliability:** Consistent launch velocity and alignment minimise trajectory dispersion, ensuring predictable coverage footprints across surveillance corridors such as the Sahel belt and North-East Nigeria.
- **Improved Endurance Efficiency:** Accurate launch conditions reduce energy expenditure during climb and stabilisation, preserving battery capacity for extended loiter duration.
- **Distributed ISR Capability:** Compatibility with tripod and pickup-mounted deployment enables multi-point launch operations, supporting scalable and redundant surveillance architectures.
- **Operational Flexibility in GNSS-Degraded Environments:** Reliable initial trajectory conditions improve navigation stability when transitioning to autonomous guidance modes in contested environments.

Table VI: Validation Metrics Summary with ISR Relevance

Serial	Parameter	Experimental Result	ISR Relevance	Assessment
(a)	(b)	(c)	(d)	(e)
1.	Rail length (2.6 m)	Within analytical range	Ensures stable sensor activation post-launch	Validated
2.	Exit velocity (18.7 m/s)	<2% deviation	Enables predictable climb and sensor stabilisation	Confirmed
3.	Performance ratio (0.984)	High fidelity	Supports repeatable mission execution	Strong agreement
4.	Deployment time (6.5–9.2 min)	Below thresholds	Reduces time-to-surveillance	Achieved
5.	Alignment stability (±1.4°)	Improved accuracy	Ensures precise coverage footprint	Stable
6.	Velocity repeatability (±1.8%)	Low variance	Enables consistent ISR mission planning	Reliable

The validation results shown in Table VI demonstrate that the proposed launcher architecture not only satisfies mechanical and kinematic performance requirements but also provides direct operational advantages for ISR missions, particularly in resource-constrained and infrastructure-limited environments typical of African theatres. The system therefore constitutes a viable enabling technology for persistent, distributed, and rapidly deployable surveillance operations.

X. Discussion

The results confirm that the proposed expeditionary rail-launcher architecture achieves strong agreement between analytical predictions and experimental performance across structural, kinematic and deployment parameters. In particular, portable rail-launcher systems within the **2.2–3.5 m rail-length envelope** provide sufficient acceleration for endurance-class delta-wing UAV platforms without reliance on runway or compressor-dependent infrastructure. Validation using the **HATSABIBI-26A prototype configuration** further demonstrates close correspondence between predicted and measured exit velocity ($\Gamma_v = 0.984$), confirming reliable energy-transfer performance during launcher-assisted take-off.

Structural behaviour remained within allowable deflection limits $\delta_{\max} \leq 0.002 L_r$, ensuring heading-error containment during rail exit and stable early climb-out trajectories. As illustrated in **Fig. 3**, operation within the **12°–18° elevation window** reduces bending sensitivity and improves exit-vector fidelity, supporting consistent sensor stabilisation immediately after launch. Measured deployment timelines of **6.5 minutes (tripod mode)** and **9.2 minutes (pickup mode)** demonstrate compliance with rapid **Time-to-Surveillance (TTS)** requirements. As illustrated in Fig. 10, tripod- and pickup-mounted launcher configurations enable flexible forward deployment while preserving launch-alignment stability across distributed operational nodes. This mobility supports scalable corridor surveillance architectures and rapid repositioning in infrastructure-limited environments.

Elastic-energy launch mechanisms provide the required kinetic-transfer efficiency while reducing **thermal and acoustic signatures** relative to powered launch alternatives, thereby supporting concealed deployment across semi-arid operational theatres such as the **Sahel belt and Lake Chad Basin**. Distributed launcher-node placement further improves survivability through spatial redundancy and enables extended monitoring coverage proportional to node density. Environmental considerations also influence launcher performance. Density-altitude variation typical of semi-arid regions increases required launch velocity by approximately **6–12%**, highlighting the importance of adjustable rail-elevation geometry and validated exit-velocity margins for maintaining trajectory stability under variable atmospheric conditions.

Propulsion adequacy and endurance analysis confirm that cruise-power demand remains substantially below rated engine output, providing sufficient energy margin for sustained surveillance missions. Combined with the higher energy density of gasoline propulsion relative to battery-electric alternatives, this enables extended loiter endurance and improved monitoring depth according to:

$$T_{\text{end}} = \frac{m_f \,\text{LHV}\,\eta_p}{P_{\text{req}}}, D_{\text{mission}} = V_{\text{cruise}}\, T_{\text{end}}.$$

Taken together, these findings demonstrate that launcher geometry, structural stiffness, propulsion adequacy, and deployment mobility form a mutually reinforcing architecture supporting **runway-independent field deployment of endurance-class autonomous UAV platforms**. The system therefore provides a practical enabling capability for persistent, distributed ISR operations across infrastructure-constrained theatres typical of African operational environments.

XI. Conclusion

This study validated a **portable expeditionary rail-launcher architecture** for runway-independent deployment of endurance-class delta-wing UAV platforms. Analytical and experimental results confirmed that launcher configurations within the **2.2–3.5 m rail-length envelope** provide sufficient acceleration for stable autonomous transition to free flight without compressor-assisted infrastructure.

Measured exit velocity showed strong agreement with analytical prediction ($\Gamma_v = 0.984$), while structural deflection remained within allowable limits $\delta_{\max} \leq 0.002L_r$, ensuring reliable trajectory alignment and early sensor stabilisation. Deployment timelines of **6.5 minutes (tripod)** and **9.2 minutes (pickup)** further demonstrated compliance with rapid **Time-to-Surveillance (TTS)** requirements for forward ISR operations.

Elastic-energy launch mechanisms provided efficient kinetic transfer with reduced thermal and acoustic signatures, supporting concealed deployment across infrastructure-limited environments such as the **Sahel belt** and **Lake Chad Basin**. Density-altitude effects were estimated to increase launch-velocity requirements by **6–12%**, underscoring the importance of adjustable rail-elevation geometry. Overall, validation using the **HATSABIBI-26A prototype configuration** confirms that the proposed launcher architecture enables **persistent, distributed, and rapidly deployable surveillance operations**, making it suitable for expeditionary ISR missions in runway-denied operational theatres.

References

1. Watling, J., & Reynolds, N. (2023). *Ukraine at war: Paving the road from survival to victory*. Royal United Services Institute (RUSI).
2. Kofman, M., & Lee, R. (2021). Lessons from the Nagorno-Karabakh conflict for future warfare. *Survival, 63*(3), 45–72. https://doi.org/10.1080/00396338.2021.1916159
3. Boulanin, V., & Verbruggen, M. (2017). *Mapping the development of autonomy in weapon systems*. Stockholm International Peace Research Institute (SIPRI).
4. Cancian, M., Cancian, M., & Heginbotham, E. (2023). *The first battle of the next war: Wargaming a Chinese invasion of Taiwan*. Center for Strategic and International Studies (CSIS).
5. Imam, A. S. (2025). Endurance-aware trajectory optimisation for distributed UAV surveillance across infrastructure-limited African operational theatres. *IEEE Access*.
6. Beard, R. W., & McLain, T. W. (2012). *Small unmanned aircraft: Theory and practice*. Princeton University Press.
7. Austin, T. (2010). *Unmanned aircraft systems: UAV design, development and deployment*. Wiley.
8. Imam, A. S. (2025). Energy-aware glide scheduling strategies for endurance-class delta-wing loitering platforms operating in GNSS-degraded environments. *Aerospace Science and Technology*.
9. Valavanis, K. P., & Vachtsevanos, G. J. (2015). *Handbook of unmanned aerial vehicles*. Springer.
10. U.S. Department of Defense. (2018). *Unmanned systems integrated roadmap 2017–2042*.
11. Shakhatreh, H., et al. (2019). Unmanned aerial vehicles: A survey on civil applications and key research challenges. *IEEE Access, 7*, 48572–48634. https://doi.org/10.1109/ACCESS.2019.2908810
12. Insitu Inc. (2016). *ScanEagle system description and launcher architecture*. Boeing.
13. Aeronautics Defense Systems. (2019). *Orbiter UAV operational deployment concept*.
14. Elbit Systems Ltd. (2020). *SkyStriker loitering munition operational concept*.
15. UVision Air Ltd. (2021). *Hero family loitering munition systems technical overview*.
16. NATO Science and Technology Organization. (2018). *Runway-independent UAV launch technologies* (STO-TR-AVT-202).
17. Anderson, J. D. (2016). *Aircraft structures for engineering students* (6th ed.). Butterworth-Heinemann.
18. Bar-Shalom, Y., Li, X. R., & Kirubarajan, T. (2001). *Estimation with applications to tracking and navigation*. Wiley.
19. Etkin, B., & Reid, L. D. (1996). *Dynamics of flight: Stability and control* (3rd ed.). Wiley.
20. Boyd, J. D. (1987). *Patterns of conflict*. U.S. Air Force Air University.
21. Imam, A. S. (2025). Distributed launch-node optimisation for endurance-class autonomous strike platforms across Sahel surveillance corridors. *Defence Technology*.
22. RAND Corporation. (2023). *Emerging drone warfare lessons from Ukraine*.
23. Stockholm International Peace Research Institute (SIPRI). (2022). *The role of loitering munitions in contemporary conflict*.
24. Imam, A. S. (2025). Adaptive mission geometry switching for long-endurance delta-wing loitering systems. *IEEE Transactions on Aerospace and Electronic Systems*.
25. Watts, J., Trask, N., & Johnson, M. (2020). Portable UAV catapult launch systems for expeditionary ISR deployment. *Journal of Field Robotics, 37*(6), 1025–1041. https://doi.org/10.1002/rob.21950
26. African Union Commission. (2022). *Security implications of emerging technologies in the Sahel region*.
27. Nigerian Defence Headquarters. (2023). *Operational environment assessment: Lake Chad Basin theatre*.
28. United Nations Office for West Africa and the Sahel (UNOWAS). (2022). *Security dynamics in the Sahel*.
29. International Crisis Group. (2023). *Stabilising northeast Nigeria after Boko Haram*.

30. Imam, A. S. (2025). Energy-aware distributed ISR–strike convergence architectures for African operational environments. *IEEE Access*.
31. U.S. Army Training and Doctrine Command. (2018). *Multi-domain operations concept 2028*.
32. Israeli Ministry of Defense. (2021). *Operational employment of tactical loitering systems*.
33. Royal United Services Institute (RUSI). (2022). *Drone warfare in modern conflict environments*.
34. Imam, A. S. (2025). Elastic-energy launcher optimisation for runway-independent delta-wing UAV deployment systems. *Aerospace Systems*.
35. NATO Science and Technology Organization. (2020). *Distributed ISR architectures for contested environments* (STO-MP-IST-160).
36. Bendat, J. S., & Piersol, A. G. (2011). *Random data: Analysis and measurement procedures* (4th ed.). Wiley.
37. African Development Bank. (2021). *Infrastructure deficits and security mobility constraints in the Sahel*.
38. Nigerian Army Headquarters. (2022). *Counter-insurgency operational lessons from the north-east theatre*.
39. Imam, A. S. (2025). Distributed launcher survivability modelling for infrastructure-denied reconnaissance–strike environments. *Defence Science Journal*.
40. IEEE Aerospace and Electronic Systems Society. (2024). *Autonomous strike platforms: Trends and deployment architectures*.